А С Т Р О Ф И З И К А

ТОМ 67 АВГУСТ, 2024 ВЫПУСК 3

DOI: 10.54503/0571-7132-2024.67.3-341

A SIMPLE ANALYTICAL METHOD USING FOKKER-PLANCK EQUATION FOR MODELING PARTICLE ACCELERATION AT ASTROPHYSICAL SHOCKS

J.-H.HA

Received 19 June 2024
Accepted 26 August 2024

Shocks are ubiquitous in astrophysical environments, and particle acceleration at such astrophysical shocks is related to high-energy phenomena. In particular, the acceleration mechanism and the time evolution of the particle distribution function have been extensively examined. This paper describes a simple analytic method using the one-dimensional Fokker-Planck equation in the test-particle regime. We aim to investigate the evolution of the particle distribution function in the shock upstream, which could be streaming toward Earth along the open magnetic field geometry. The behavior of the analytical solution is examined over a wide range of parameters representing shock structure, such as the shock Mach number, plasma beta, injection fraction into diffusive shock acceleration, and the scale of the upstream magnetic field. The behavior is associated with upstream turbulence for diffusive shock acceleration, as expected. Additionally, pre-accelerated particles could affect the time evolution of the particle distribution only when the radiative or advection losses are small enough for the pre-accelerated distribution to have a flatter power-law slope than the power-law slope based on shock acceleration theory. We also provide a formula for a spherically expanding shock and its relevant application to calculate high-energy emission due to hadronic interactions. We suggest that the simple analytic method could be applied to examine astrophysical shocks with a wide range of plasma parameters.

Keywords: *particle acceleration: high-energy radiation: astrophysical shocks: Fokker-Planck equation*

1. *Introduction.* Shocks are induced in various astrophysical environments due to supersonic flow motions such as coronal mass ejections in the interplanetary medium [1-3], supernova remnants in the interstellar medium [4-6], and gravitational collapse in the large-scale structure of the universe [7-10]. While the properties of shocks can be affected by the characteristics of the medium, it has been demonstrated that such shocks efficiently accelerate particles. Particle acceleration at shocks has been explained by first-order Fermi acceleration, which states that particles can gain energy through multiple interactions with the converging waves near the shocks (i.e., diffusive shock acceleration (DSA, hereafter)) [11,12]. Modeling particle acceleration at astrophysical shocks has been examined by previous studies using numerical approaches, including plasma kinetic simulations [13-18], hydrodynamic simulations [19,20], and models for the advection-diffusion

of particle distribution functions in spatial and momentum space based on the Fokker-Planck equation [1,20-23].

Using plasma kinetic simulations, the physical mechanisms for magnetic field amplification and wave generation for scattering off particles in both the upstream and downstream regions have been extensively studied [13-18]. Although the properties of plasma waves for particle acceleration can depend on the characteristics of the medium, such as supersonic flow properties (i.e., nonrelativistic, relativistic) and magnetic field strength (i.e., unmagnetized, weakly magnetized, and strongly magnetized plasmas), it has been shown that plasma waves can be induced by various instabilities due to the plasma beam distribution causing velocity space anisotropy [16,17]. According to simulation results, such waves can be self-excited due to particle reflection at the shock surface during the evolution of collisionless shocks, and evidence of particle acceleration through multiple wave-particle interactions has been observed [13-15,18]. While plasma kinetic simulations are a powerful tool for investigating the microphysics of particle acceleration through first-principle calculations, they are limited in their ability to observe the full DSA process, which occurs over longer timescales than the growth timescale of plasma instabilities.

Considering the effects of particle acceleration at shocks and their observational implications beyond the kinetic scales, theoretical modeling has been conducted, including DSA-produced cosmic-ray populations (i.e., cosmic-ray populations following a power-law distribution) and the physics of advection and diffusion in spatial and momentum spaces. To obtain the particle spectral evolution as a stationary shock structure, a test-particle approach has been employed, assuming that the evolution of the shock structure is independent of the dynamical feedback of cosmic-ray particles [1,23]. Moreover, hydrodynamic simulations, including magnetohydrodynamics, have been used to model the dynamical evolution of shocks in astrophysical media more sophisticatedly [9,10,24,25]. Based on such modeling, multi-wavelength emissions due to particle acceleration at shocks have also been examined [24-29].

As a follow-up to the previous studies summarized above, this study aims to describe simplified analytic method using the one-dimensional Fokker-Planck equation. The effects of shock upstream conditions on particle spectral evolution were also examined to demonstrate the robustness of the analytical solution in various astrophysical environments. Additionally, we provide a potential application for calculating high-energy radiation due to particle acceleration at shocks, showing that our simple model can be used as a tool for rapidly estimating observable radiation flux. Moreover, the simple analytical approach described in this work has the advantage of being flexibly expandable. In particular, it would be possible to extend our simple model to incorporate detailed physics, including diffusion models and the microphysics of particle injection into DSA.

2. *Basic physics*. This section describes the basic physics, including the particle distribution function and relevant plasma physics, for particle acceleration at collisionless shocks. The importance of the characteristics of the particle distribution function for estimating the efficiency of particle acceleration at shocks is also discussed.

2.1. *Particle distribution function*. The particle distribution of thermal plasma is commonly modeled as Maxwellian, given by

$$f_{MW}(p) = \frac{n_{0i}}{\pi^{3/2}} p_{th}^{-3} \exp\left[-\left(\frac{p}{p_{th}}\right)^2\right], \tag{1}$$

where $p_{th} = \sqrt{2mk_BT}$ is the thermal momentum and n_{0i} is the plasma density, defined as

$$n_{i0} \equiv \int 4\pi p^2 f_{MW}(p) dp. \tag{2}$$

While the Maxwellian distribution is reasonable for describing the medium in the absence of nonlinear processes such as plasma and magnetohydrodynamic (MHD) waves, shocks, and turbulence, it has been demonstrated that plasma processes associated with such phenomena can accelerate particles. This particle energization results in a particle distribution that deviates from the Maxwellian, known as the kappa distribution [30-32]. The kappa distribution is defined as:

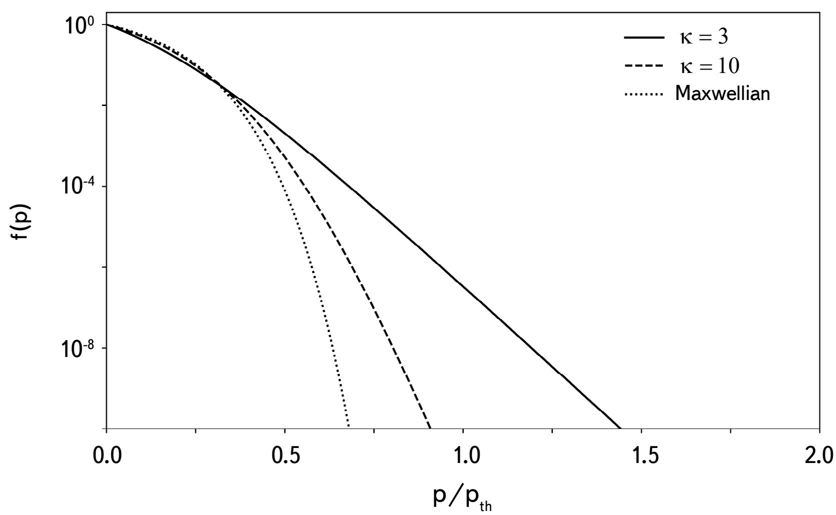

Fig.1. Examples of Maxwellian and kappa distribution functions.

$$f_\kappa(p)=\frac{n_{0i}}{\pi^{3/2}}p_{th}^{-3}\frac{\Gamma(\kappa+1)}{(\kappa-3/2)^{3/2}\Gamma(\kappa-1/2)}\left[1+\frac{1}{(\kappa-3/2)}\left(\frac{p}{p_{th}}\right)^2\right]^{-(\kappa+1)}, \tag{3}$$

where $\Gamma(x)$ is the Gamma function and the parameter, κ, determines the slope of the supra-thermal distribution. For $p >> p_{th}$, the kappa distribution follows a power-law form, $f_\kappa(p) \propto p^{-2(\kappa+1)}$. Fig.1 shows examples of particle distribution functions. A smaller value of κ results in a flatter particle distribution, whereas a larger value of κ makes the kappa distribution closer to the Maxwellian. It has been shown that the kappa distribution modulates the nature of plasma waves [33], and thus the presence of such suprathermal populations could affect the efficiency of shock acceleration.

2.2. *Plasma physics for particle acceleration at collisionless shocks*. To understand particle acceleration at shocks mediated by waves in the shock upstream and downstream, the evolution of shock structure and the plasma instabilities responsible for generating plasma waves that scatter off particles should be considered. When examining plasma processes associated with electrostatic waves, plasma frequencies ($\omega_{pe}=\sqrt{4\pi ne^2/m_e}$, $\omega_{pi}=\sqrt{4\pi ne^2/m_i}$) and skin depths ($c/\omega_{pe}$ and c/ω_{pi}) are employed. Electromagnetic interactions, on the other hand, are characterized using gyrofrequencies ($\Omega_e=eB/m_ec$, $\Omega_i=eB/m_ic$) and gyroradii of thermal electrons and ions ($r_{th,e}=v_{th,e}/\Omega_e$, $r_{th,i}=v_{th,i}/\Omega_i$). Particularly, the characteristic scales of ions (i.e., Ω_i^{-1}, $r_{th,i}$) are employed to describe the dynamics of shock evolution, where the shock thickness is a few times the gyroradius of downstream thermal ions, $r_{th,i2}$. This indicates that particle energization through multiple crossings of the shock structure (i.e., diffusive shock acceleration, DSA) is feasible only for particles with momenta greater than the so-called injection momentum, $p_{inj}\sim 3p_{th,i2}=3\sqrt{2m_ik_BT_2}$ [16,19,34-35]. It has been demonstrated that particles with momenta beyond p_{inj} drive plasma instabilities in the shock upstream and downstream, and these self-excited plasma waves can further accelerate particles [13-18]. Plasma kinetic simulations have provided evidence that such plasma processes can extend to DSA [13-15,18].

When modeling the distribution of shock-accelerated particles, the number of particles with $p \geq p_{inj}$ is parameterized as the so-called injection fraction, ε_{inj}. It is important to note that this injection fraction can strongly depend on the distribution of the background medium. If shock acceleration and particle transport associated with MHD waves are active in the medium, the thermal particle distribution may deviate from the Maxwellian distribution and instead follow the kappa distribution. Specifically, the presence of a kappa distribution could enhance the injection fraction, as illustrated in Fig.2.

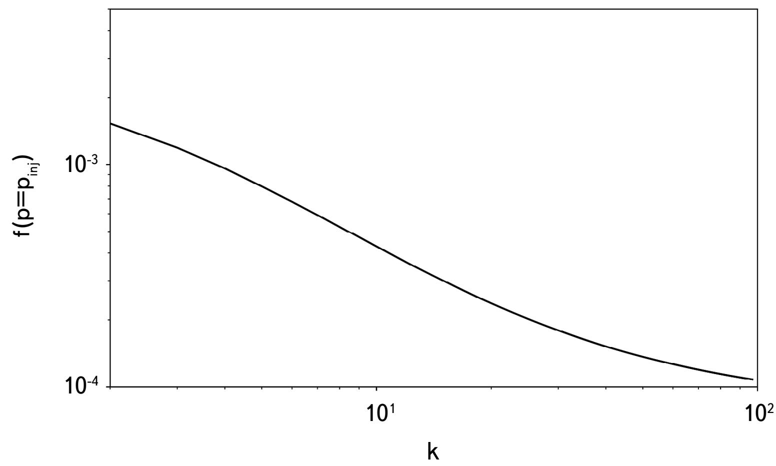

Fig.2. The normalization of the particle distribution function at $p = p_{inj}$ with different kappa values ranging from $\kappa = 2$ to $\kappa = 10^2$.

In the modeling described in the following section, two main factors of the kappa distribution were considered: (1) the injection fraction into DSA, which changes the efficiency of shock acceleration; and (2) the effects of the momentum distribution of pre-accelerated particles following a power-law form.

3. *Simple analytic model based on Fokker-Planck equation.*

3.1. *Shock structure and one-dimensional Fokker-Planck equation.* In this work, we solve the Fokker-Planck equation to study the time evolution of shock-accelerated particles due to diffusive shock acceleration (DSA). Throughout the paper, we use formulas in the shock rest frame. Considering the scale length of the magnetized medium, $L_B = B(\partial B/\partial r)^{-1}$ with an open field geometry in the shock upstream $B_1(r) = B_0 \exp(-r/L_B)$, we assume the shock structure as follows:

$$
\begin{aligned}
U(r) &\approx \begin{cases} U_1, & r>0, \\ U_2 = U_1/\rho_c, & r<0, \end{cases} \\
n(r) &\approx \begin{cases} n_1 = n_{i0}\exp(-2r/L_B), & r>0, \\ n_2 = \rho_c\, n_{i0}, & r<0, \end{cases} \\
B(r) &\approx \begin{cases} B_1 = B_0\exp(-r/L_B), & r>0, \\ B_2 = \rho_c\, B_0, & r<0, \end{cases} \\
T(r) &\approx \begin{cases} T_1, & r>0, \\ T_2, & r<0, \end{cases}
\end{aligned}
\tag{4}
$$

where $U(r)$, $n(r)$, $B(r)$ and $T(r)$ represent the velocity, density, magnetic field, and temperature profiles, respectively, and ρ_c denotes the shock compression ratio. The subscripts 1 and 2 denote upstream and downstream quantities, respectively. The sonic and Alfvenic Mach numbers are then calculated as follows:

$$M_s = \frac{U_1}{c_s}, \quad M_A = \frac{U_1}{V_A} = \sqrt{\frac{\gamma\beta}{2}} M_s, \tag{5}$$

where $c_s = \sqrt{2\gamma n_i k_B T_1 / m_i}$ and $V_A = B_0 / \sqrt{4\pi n_i m_i}$ are the sound and Alfven speeds, respectively, with the adiabatic index, $\gamma = 5/3$. According to the shock jump condition, the temperature jump can be computed using the sonic Mach number:

$$\frac{T_2}{T_1} = \frac{\left(5M_s^2 - 1\right)\left(M_s^2 + 3\right)}{16 M_s^2}. \tag{6}$$

In the finite shock upstream and downstream, the spatial diffusion coefficients associated with the plasma waves are defined as:

$$D(r) = \begin{cases} D_1(p), & L_1 > r > 0, \\ D_2(p), & -L_2 < r < 0, \end{cases} \tag{7}$$

where L_1, and L_2 represent the finite sizes of the shock upstream and downstream, respectively.

Since the DSA process can be explained in a one-dimensional system, we solved the one-dimensional Fokker-Planck equation. To account for the advection and diffusion of particle distribution into the interplanetary and interstellar medium, characterized by an open field geometry, we solved the one-dimensional Fokker-Planck equation in the shock upstream, as follows:

$$\begin{aligned} &\frac{\partial f(r,p,t)}{\partial t} + \frac{\partial}{\partial r}\left(U_1 + \frac{D_1(p)}{L_B}\right) f(r,p,t) - \left(\frac{\partial U_1}{\partial r} + \frac{U_1}{L_B}\right)\frac{\partial}{\partial p}\frac{p}{3} f(r,p,t) \\ &\qquad - \frac{\partial}{\partial r}\left(D_1(p)\frac{\partial f(r,p,t)}{\partial r}\right) = s(r,p,t), \end{aligned} \tag{8}$$

where $f(r,p,t)$ and $s(r,p,t)$ denote the particle distribution function and the source function, respectively. Based on the DSA theory and assuming steady injection, the initial particle distribution $f_0(r,p,t=0)$, and the source term $s(r,p,t)$ are assumed as follows:

$$\begin{aligned} Q_{inj}(r) &= \varepsilon_{inj}\, n_{i,0} U_1 \exp\left(-\frac{2r}{L_B}\right), \\ f_0(r,p,t=0) &= \frac{Q_{inj}(r)}{4\pi U_1 p_{inj}^3}\left(\frac{p}{p_{inj}}\right)^{-q} = \frac{\varepsilon_{inj}\, n_{i,0}}{4\pi\, p_{inj}^3}\exp\left(-\frac{2r}{L_B}\right)\left(\frac{p}{p_{inj}}\right)^{-q}\exp\left(-\frac{p}{p_{max}}\right), \\ s(r,p,t) &= Q_{inj}(r)\delta(r)\delta\left(p - p_{inj}\right) = \varepsilon_{inj}\, n_{1,0} U_1 \exp\left(-\frac{2r}{L_B}\right)\delta(r)\delta\left(p - p_{inj}\right), \end{aligned} \tag{9}$$

where p_{inj} and p_{max} are the injection and maximum momentum, respectively. As described in the section 2.2, the injection momentum is approximately a few times of the downstream thermal momentum, $p_{inj} \sim 3\, p_{th,i2} = 3\sqrt{2 m_i k_B T_2}$. Considering the gyroradius of particles, the maximum momentum can be constrained by the size of the magnetic field of the system, $p_{max}c/eB_0 \approx L_B$. In addition, ε_{inj} denotes the injection fraction into DSA.

We here derive a simplified analytic form of $\partial f/\partial t$ at the shock front based on the shock structure described above in the test-particle limit. Adopting the exponential shock precursor defined in Eqs. (4) and (7), we obtained the following derivatives of $f \propto n_{i0}\exp(-2r/L_B)$ in the spatial domain:

$$\frac{\partial f}{\partial r} \approx -\frac{2}{L_B} f\,, \quad \frac{\partial^2 f}{\partial r^2} \approx \frac{4}{L_B^2} f\,, \quad \frac{\partial U_1}{\partial r} \approx 0\,, \quad \frac{\partial D_1}{\partial r} \approx 0\,. \tag{10}$$

We also obtain the following derivative of $f \propto p^{-q}$,

$$\frac{\partial (pf)}{\partial p} = (1-q) f\,. \tag{11}$$

Using Eqs. (10)-(11), the partial derivative terms of Eq. (8) can be simplified at the shock front as follows:

$$\begin{gathered}
\frac{\partial}{\partial r}\left(U_1 + \frac{D_1(p)}{L_B}\right) f(r,p,t) \approx \left(U_1 + \frac{D_1(p)}{L_B}\right)\frac{\partial f(r,p,t)}{\partial r} = -\left(\frac{2U_1}{L_B} + \frac{2D_1(p)}{L_B^2}\right) f(r,p,t), \\
\left(\frac{\partial U_1}{\partial r} + \frac{U_1}{L_B}\right)\frac{\partial}{\partial p}\frac{p}{3} f(r,p,t) \approx \frac{U_1}{L_B}\frac{\partial}{\partial p}\frac{p}{3} f(r,p,t) = \frac{U_1}{L_B}\frac{1-q}{3} f(r,p,t), \\
\frac{\partial}{\partial r}\left(D_1(p)\frac{\partial f(r,p,t)}{\partial r}\right) \approx D_1(p)\frac{\partial^2 f(r,p,t)}{\partial r^2} = \frac{4D_1(p)}{L_B^2} f(r,p,t).
\end{gathered} \tag{12}$$

Based on Eqs. (12), $\partial f/\partial t$ can be simplified as

$$\frac{\partial f(r,p,t)}{\partial t} \approx -\left(\frac{7-q}{3}\frac{U_1}{L_B}\right) f(r,p,t) + \frac{6D_1(p)}{L_B^2} f(r,p,t) + s(r,p,t). \tag{13}$$

Here, the first and second terms denote the contributions of advection and diffusion, respectively. The time evolution of $f(r,p,t)$ is then computed numerically as follows,

$$\begin{aligned}
f(r,p,t_{i+1}) = f(r,p,t_0) + \int_0^{t_i} \left(\frac{\partial f(r,p,t)}{\partial t}\right)_{t_i} dt = f(r,p,t_0) \\
+ \sum_{t_i \in \{0,\, \tau_{acc}\}} \Delta t \left(\frac{\partial f(r,p,t)}{\partial t}\right)_{t_i}\,.
\end{aligned} \tag{14}$$

Here, time interval Δt satisfies $\Delta t << \tau_{acc}$ and is normalized in units of Ω_i^{-1}, since the acceleration timescale depends on Ω_i^{-1}.

3.2. *Characteristic scales*. To calculate the accumulated particle distribution function, the following characteristic timescales are employed:

$$\tau_{AD} \approx \frac{L_1}{U_1},$$
$$\tau_{acc}(p) \approx \frac{1}{U_1 - U_2}\left[\frac{D_1(p)}{U_1} + \frac{D_2(p)}{U_2}\right] \approx \frac{D_1(p)}{U_1^2}\left(\frac{1}{1-\rho_c^{-1}}\right)\left(\frac{1}{1+\rho_c^2}\right),$$
$$\tau_{diff}(p) \approx \frac{D_1(p)}{U_1^2} \approx \frac{2}{\pi}\frac{1}{q}\left(\frac{M_A - 1}{\varepsilon_{inj} M_A^2}\right)\left(\frac{p}{p_{inj}}\right)^{q-3} \Omega_i^{-1}, \tag{15}$$
$$D_1(p) \approx \frac{1}{3}\nu\lambda_1(p) \approx \frac{2}{\pi}\frac{1}{q}\left(\frac{M_A - 1}{\varepsilon_{inj} M_A^2}\right)\left(\frac{p}{p_{inj}}\right)^{q-3} U_1^2\, \Omega_i^{-1}.$$

Here, τ_{AD} is the adiabatic deceleration timescale of a supersonic ejecta, τ_{acc} is the shock acceleration timescale, and τ_{diff} is the turbulent diffusion timescale associated with waves generated by shock-accelerated particles [3]. In 2-nd Eq. of (15), the acceleration timescale satisfies $\tau_{acc} < \tau_{diff}$ since the shock compression ratio ρ_c is always larger than 1. This is consistent with the physical requirement that the timescale for particle acceleration should be shorter than the diffusion timescale; otherwise, particles would diffuse away from the shock surface before undergoing significant acceleration. Additionally, adiabatic losses typically occur more slowly than diffusion and acceleration processes. The relationship between characteristic timescales and length scales (i.e., $L_{diff} \approx U_1 \tau_{diff}$, $L_{acc} \approx U_1 \tau_{acc}$ and $L_1 \approx U_1 \tau_{AD}$) can be summarized as follows, particularly for particles with $p \le p_{max}$:

$$\tau_{acc}(p) < \tau_{diff}(p) << \tau_{AD}, \quad L_{acc}(p) < L_{diff}(p) << L_1. \tag{16}$$

In panel (a) of Fig.3., we plot the characteristic length scales with the following parameters: $\beta = 1$, $M_s = 5$, $M_A = 4.56$, $c_s/c = 10^{-4}$, $V_A/c = 1.09 \cdot 10^{-4}$, $\varepsilon_{inj} = 10^{-2}$. Throughout the entire momentum domain, L_{acc} exceeds L_{diff}. Given the finite system size where $L_1 \approx L_B$, particle momentum can reach up to p_{max}. Beyond p_{max}, particles cannot be further energized through DSA due to the absence of plasma waves with wavelengths larger than $\lambda_w \approx L_B$. In the remaining panels of Fig.3, we analyze the diffusion length scale by varying the sonic Mach number, M_s (panel (b)), the injection fraction into DSA, ε_{inj} (panel (c)) and plasma beta, β (panel (d)). As shown in panel (b), the diffusion length is longer for smaller M_s, reflecting a steeper slope of $f(x, p, t)$ beyond p_{inj}, which can reduce instabilities associated with high-energy particle streaming [11,36,37]. Similarly, panel (c) shows that the diffusion length depends on ε_{inj}. In panel (d), we observe that the diffusion length scale increases with β because higher β values indicate lower magnetic energy in plasma waves. Notably, the diffusion length converges at sufficiently high β

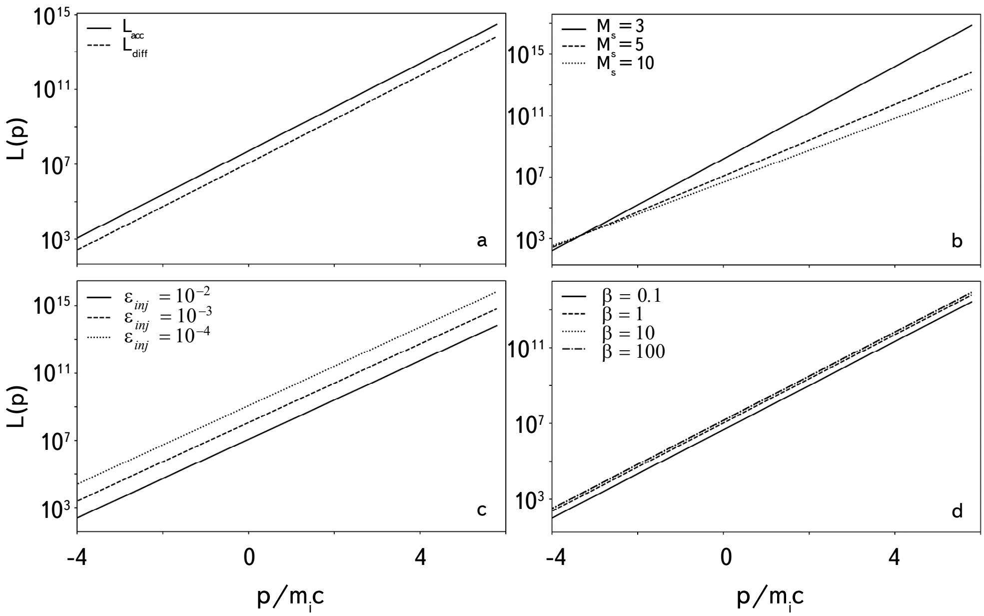

Fig.3. (a) Acceleration length scale (solid line) and diffusion length scale (dashed line) using the parameters with $\beta = 1$, $M_s = 5$, $M_A = 4.56$, $c_s / c = 10^{-4}$, $V_A / c = 1.09 \cdot 10^{-4}$, $\varepsilon_{inj} = 10^{-2}$; (b) Diffusion length scales with different sonic Mach numbers; (c) Diffusion length scales with different injection rates; (d) Diffusion length scales with different plasma betas. In panels (b) - (d), the same parameters used in panel (a) were employed except for the parameter being investigated for dependency.

($\beta >> 1$). This convergence occurs because in very weakly magnetized plasma, particle dynamics are largely influenced by self-excited magnetic fields due to high-energy particle streaming. This behavior aligns with 3-rd Eq. of (15), where for $\beta >> 1$, the diffusion length $L_{diff}(p)$ approximates:

$$L_{diff}(p) \sim \frac{D_1(p)}{U_1} \propto \frac{\Omega_i^{-1}}{M_A}. \tag{17}$$

Given $\Omega_i^{-1} \to \infty$ and $M_A \to \infty$ as $\beta \to \infty$, $L_{diff}(p)$ converges accordingly.

3.3. *Effects of shock parameters on the particle distribution function*. In this section, we present the analytic solution of the one-dimensional equation, including the time evolution of the particle distribution and its parameter dependencies such as the sonic Mach number M_s, the injection fraction ε_{inj}, plasma beta β, and the scale length L_B (or p_{max}). Such an investigation across the parameter space provides reliability to the analytic solution in tracking the time evolution of shock-accelerated particles. Table 1 summarizes the parameters used in this paper. Velocities are expressed in units of the speed of light c, and the scale length L_B, is normalized by $10^2\, r_{i,th}$, considering that plasma processes at the shock structure could pre-accelerate particles up to $pc/eB_0 \sim 10^2\, r_{i,th}$ [13-15].

Table 1

PARAMETERS USED IN THIS WORK.

Case 1 is the fiducial case and the remaining cases are performed for comparison. Groups for particular parameter dependence are summarized as follows: (L_B: Case1, Case2, Case3); (M_s: Case1, Case4, Case5); (ε_{inj} : Case1, Case6, Case7); (β: Case1, Case8, Case9, Case10).

	β	M_s	M_A	c_s/c	V_A/c	ε_{inj}	$L_B/(10^2 r_{i,th})$
Case1	1	5	4.56	10^{-4}	$1.09 \cdot 10^{-4}$	10^{-2}	10^3
Case2	1	5	4.56	10^{-4}	$1.09 \cdot 10^{-4}$	10^{-2}	10^5
Case3	1	5	4.56	10^{-4}	$1.09 \cdot 10^{-4}$	10^{-2}	10^{10}
Case4	1	3	2.74	10^{-4}	$1.09 \cdot 10^{-4}$	10^{-2}	10^{10}
Case5	1	10	9.13	10^{-4}	$1.09 \cdot 10^{-4}$	10^{-2}	10^{10}
Case6	1	5	4.56	10^{-4}	$1.09 \cdot 10^{-4}$	10^{-3}	10^{10}
Case7	1	5	4.56	10^{-4}	$1.09 \cdot 10^{-4}$	10^{-4}	10^{10}
Case8	0.1	5	1.44	10^{-4}	$3.45 \cdot 10^{-4}$	10^{-2}	10^3
Case9	10	5	14.42	10^{-4}	$3.45 \cdot 10^{-5}$	10^{-2}	10^3
Case10	100	5	45.64	10^{-4}	$1.09 \cdot 10^{-5}$	10^{-2}	10^3

We first examine the time evolution of the particle distribution function at the shock front shown in Fig.4. Each line in the plot represents a time interval of 250 Ω_i^{-1}, which is sufficient to capture the plasma processes of DSA [13,14]. While the slope of the distribution function remains constant, momentum diffusion is observed as a consequence of continuous energy injection from the source term, $s(r, p, t)$. At $t = t_3$, particles accumulate near $p/m_i c \sim 10^3$ due to the limited scale of the magnetic field size L_B in the shock upstream. Such particles could escape from the shock structure and be observed as galactic or extragalactic cosmic rays.

We next investigate how the particle distribution function at the shock front depends on the parameters (i.e., M_s, ε_{inj} , β, L_B). Fig.5 displays the momentum distribution functions at the shock front at $t = t_1 = 500\Omega_i^{-1}$ with a wide range of parameters. The panels illustrate that M_s and ε_{inj} affect the slope and normalization of the particle distribution function, respectively, as shown in panels (a) and (b), especially when the magnetic scale L_B is sufficiently large. The dependence on L_B shown in panel (c) indicates that the spectra with larger L_B can extend to higher momenta. We particularly focus on the dependence of β with the same L_B. With the same system size, the maximum momentum gained via DSA is proportional to the magnetic field because the gyroradius of particles increases with decreasing magnetic field strength. The time-evolved spectra with different values of plasma beta shown in panel (d) are consistent with this interpretation. If the system size and the wavelength of upstream waves were infinite, such beta dependence would not be observed.

3.4. *Effects of pre-accelerated particles*. We now expand the analytic solution to include pre-accelerated particles influenced by shocks or turbulence. These pre-accelerated particles, following power-law distribution, can undergo

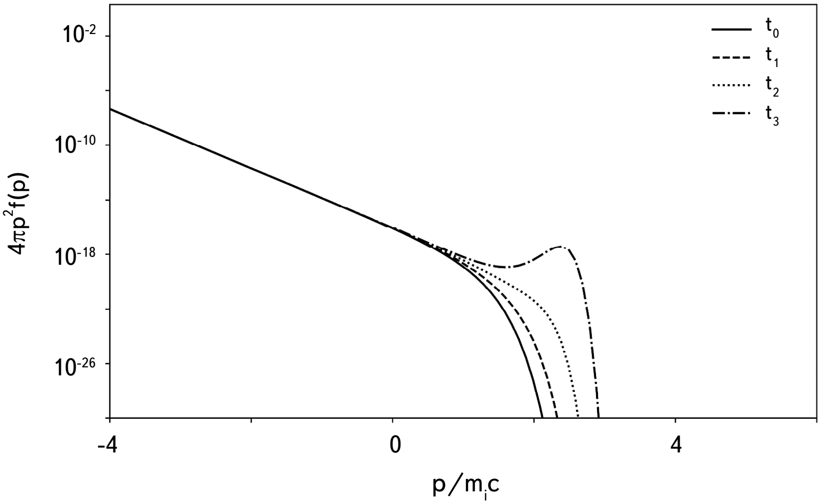

Fig.4. Time evolution of the particle distribution function at the shock front (Case 1 in Table 1). The plots are shown from $t_0 = 250\,\Omega_i^{-1}$ to $t_3 = 1000\,\Omega_i^{-1}$ with a time interval of $250\,\Omega_i^{-1}$.

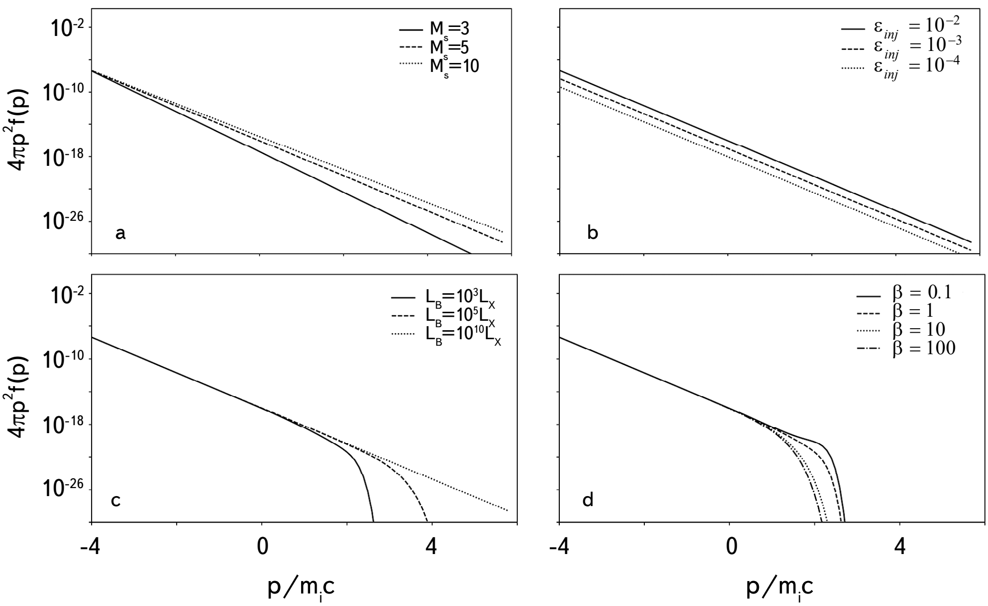

Fig.5. (a) Dependence on the sonic Mach number; (b) Dependence on the injection fraction; (c) Dependence on the magnetic field size; (d) Dependence on the plasma beta. The model information is provided in Table 1. Note that the particle distribution functions are measured at the shock front.

further acceleration through DSA [39,40]. The initial particle distribution, including the shock-accelerated particle distribution, $\tilde{f}(r, p, t=0)$, can be summarized as follows:

$$Q_{pre}(r) = \varepsilon_{pre}\, n_{i,0} U_1 \exp\left(-\frac{2r}{L_B}\right),$$

$$f_{pre}(r, p, t=0) = \frac{Q_{pre}(r)}{4\pi U_1 p_{inj}^3}\left(\frac{p}{p_{inj}}\right)^{-\tilde{q}} = \frac{\varepsilon_{pre}\, n_{i,0}}{4\pi\, p_{inj}^3}\exp\left(-\frac{2r}{L_B}\right)\left(\frac{p}{p_{inj}}\right)^{-\tilde{q}},$$

$$\tilde{f}(r, p, t=0) = \frac{Q_{inj}(r)}{4\pi U_1 p_{inj}^3}\left(\frac{p}{p_{inj}}\right)^{-q} + q p^{-q}\int_{p_{inj}}^{p} p'^{q-1} f_{pre}(r, p, t=0)\, dp' \tag{18}$$

$$= \frac{Q_{inj}(r)}{4\pi U_1 p_{inj}^3}\left(\frac{p}{p_{inj}}\right)^{-q} + \frac{q}{(q-\tilde{q})}\left(1-\left(\frac{p}{p_{inj}}\right)^{-(q-\tilde{q})}\right)\frac{Q_{pre}(r)}{4\pi U_1 p_{inj}^3}\left(\frac{p}{p_{inj}}\right)^{-\tilde{q}},$$

where ε_{pre} is a parameter that determines the normalization of the pre-accelerated distribution, $f_{pre}(r, p, t=0)$. We particularly consider the cases where $q \neq \tilde{q}$. For $q < \tilde{q}$, the pre-accelerated distribution is steeper than the DSA slope, indicating that radiative or advection losses dominate over diffusion processes in confining particles near the shock surface. For $q > \tilde{q}$, on the other hand, strong turbulence exists to confine the pre-accelerated particles.

Using the parameter set from Case 1 in Table 1, we examined the impact of pre-accelerated particles on the time evolution of the particle distribution function at the shock front by varying the parameters, $\tilde{q}$, and ε_{pre}. For reference, the particle distribution function generated by the shock with $M_s = 5$ exhibits the slope, $q = 4.17$. The dependence on the slope of pre-accelerated particles, $\tilde{q}$, is shown in Fig.6 for four different timesteps ($t = [t_0, t_3]$). Here, the normalization factor is assumed as $\varepsilon_{pre}/\varepsilon_{inj} = 10^{-1}$. The results demonstrate that the effects of pre-accelerated particles are significant when the pre-accelerated distribution has a flatter slope than the DSA slope ($q > \tilde{q}$). Conversely, when $q < \tilde{q}$, the contribution of pre-accelerated particles appears negligible. Consistently, the time-evolved particle distribution function exhibits a power-law slope q, independent of $\tilde{q}$, as shown in previous studies [40]. Furthermore, the dependence on the number density of pre-accelerated particles, $\varepsilon_{pre}/\varepsilon_{inj}$, ranging from 10^{-3} to 10^{-1} with $\tilde{q} = 4$, is shown in Fig.7. As expected, $\varepsilon_{pre}/\varepsilon_{inj}$ influences the slope of the time-evolved distribution function.

The effects of pre-accelerated particles can be applied to analyze various astrophysical environments. For instance, in galaxy clusters, multiple shocks with different Mach numbers M_s are continuously induced due to gravitational collapse, enabling particle acceleration through these shocks. Ha et al. [24], for example,

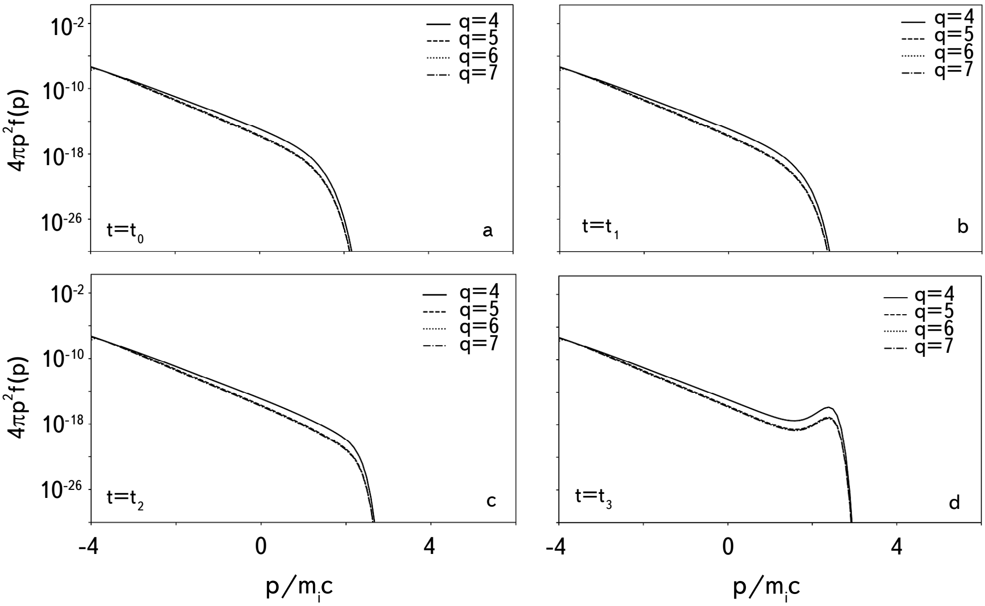

Fig.6. Time evolution of the particle distribution function at the shock front for different values of $\tilde{q}$, ranging from 4 to 7.

calculated accumulated cosmic ray spectra without considering the detailed time evolution of particle spectra. Furthermore, in star-forming galaxies, numerous shocks are generated by stellar winds and supernova remnants. We interpret that multiple acceleration processes could be active in such environments.

3.5. *Applications*. We interpret that the simple solution of the Fokker-Planck equation could be applicable to typical astrophysical shocks propagating in interplanetary, interstellar, and intracluster media. It is shown that this simple solution demonstrates reliable parameter dependence regarding particle acceleration via DSA. Once the shock parameters are obtained from observational data, the averaged particle distribution function over time and spatial domains can be computed. We provide an example assuming a spherically expanding shock with the shock surface, $A_s(t) \approx \Theta_s(r_s(t))^2$, where Θ_s is the solid angle and $r_s(t)$ is the mean shock propagation length at time t. Using the volume that the shock passed through, the volume-averaged distribution function, $\bar{f}(p)$, can be calculated as follows:

$$\bar{f}(p) \approx \frac{\sum_{t_i \in \{0,\tau_{acc}\}} A_s(t_i) U_2 f(r, p, t_i) \Delta t}{\sum_{t_i \in \{0,\tau_{acc}\}} A_s(t_i) U_2 \, \Delta t} . \tag{19}$$

For shocks in the interplanetary medium, for example, the shock parameters

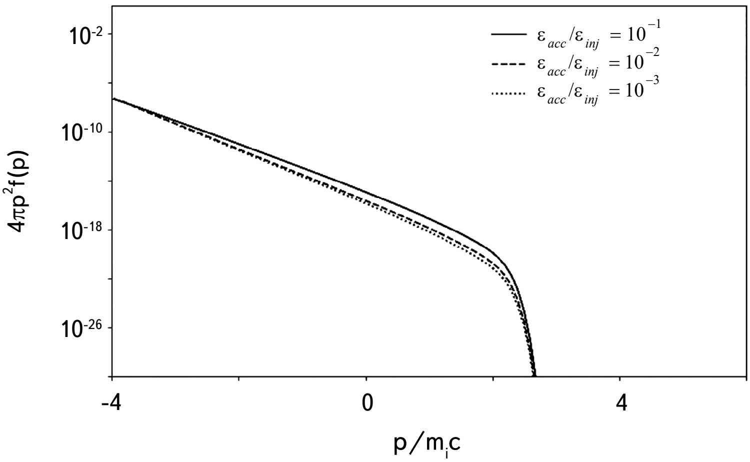

Fig.7. Effect of the fraction of pre-accelerated particles at the shock front, $\varepsilon_{pre}/\varepsilon_{inj}$ at $t = t_2$.

associated with coronal mass ejections (CME) can be obtained using publicly available IDL tools (such as the CME Analysis Tool; see [38]). By adopting the solid angle and speed of CME along with solar wind parameters such as density and magnetic fields, it is possible to estimate the averaged particle flux that could impact space weather.

The analytic solution can be also used to calculate high-energy radiation. For instance, hadronic γ-rays resulting from inelastic collisions between shock-accelerated protons and background thermal protons have been observed from supernova remnants [41,42] and star-forming galaxies [43-46]. Using the volume-averaged particle distribution function, $\bar{f}(p)$, with the dynamical timescale of the shock, τ_{dyn}, the number density of shock-accelerated particles, $N_i(E)$, can be computed as follows:

$$\frac{N_i(p)}{\tau_{dyn}} \sim \bar{f}(p), \quad N_i(E) = 4\pi p^2 N_i(p) \frac{dp}{dE}. \tag{20}$$

The pion source function is computed using the following equation proposed by Kelner et al. [47]:

$$\begin{gathered} N_\pi(E_\pi) = \frac{c n_m}{K_\pi} \sigma_{pp}\left(m_i c^2 + \frac{E_\pi}{K_\pi}\right) N_i\left(m_i c^2 + \frac{E_\pi}{K_\pi}\right), \\ \sigma_{pp}(E) = \left(34.3 + 1.88\theta + 0.25\theta^2\right)\left[1 - \left(\frac{E_{th}}{E}\right)^4\right]^2 mb, \end{gathered} \tag{21}$$

where $K_\pi \sim 0.17$ is the fraction of kinetic energy transferred from a proton to a pion, n_m is the number density of the background medium, and $\sigma_{pp}(E)$ is the cross-section of proton-proton collisions with $\theta = \ln(E/\mathrm{TeV})$, and the threshold energy, $E_{th} = 1.22\,\mathrm{GeV}$. Using the pion source function, the γ-ray production rate is then calculated as:

$$N_\gamma(E_\gamma) = 2\int_{E_{min}}^{\infty} \frac{N_\pi(E_\pi)}{\sqrt{E_\pi^2 - m_\pi^2 c^4}}\, dE_\pi\,, \tag{22}$$

where $E_{min} = E_\gamma + m_\pi^2 c^4 / (4E_\gamma)$ is the minimum energy of the produced γ-ray. Previous studies for estimating hadronic γ-ray from extragalactic sources typically assume a steady-state particle distribution function produced at shock to calculate the accumulated cosmic-ray flux during the system's dynamical timescales [26-29]. Since the simple model formulated in this paper includes the time evolution of the particle distribution function, it would be possible to improve such models by incorporating this time evolution. We will leave these investigations for future work.

4. *Summary*. In this study, we developed an analytic method using the one-dimensional Fokker-Planck equation to examine the time evolution of particle distribution functions at the shock front in the context of diffusive shock acceleration (DSA). We explored the impact of various shock parameters, including the sonic Mach number M_s, injection fraction ε_{inj}, plasma beta β, and scale length L_B. Our findings demonstrated the reliability of the analytic solution in capturing the time-dependent behavior of shock-accelerated particles, highlighting the interplay between advection, diffusion, and injection processes. The results showed that the momentum diffusion and particle accumulation are significantly influenced by these parameters, providing valuable insights into the particle acceleration mechanisms in astrophysical environments.

Additionally, we extended our model to include the effects of pre-accelerated particles, revealing that the initial distribution of these particles can alter the subsequent DSA process. We applied our model to various astrophysical scenarios, such as galaxy clusters and star-forming galaxies, where multiple shocks and turbulence are prevalent. Furthermore, the analytic solution was utilized to calculate high-energy radiation, specifically hadronic γ-rays produced by inelastic collisions between shock-accelerated protons and background thermal protons. By incorporating the time evolution of the particle distribution function, our model offers improvements over traditional steady-state approaches, laying the foundation for more accurate predictions of cosmic-ray spectra and high-energy radiation in diverse astrophysical contexts.

Acknowledgements. We thank to anonymous referees for providing constructive comments to improve the manuscript.

Korea Space Weather Center, Korea AeroSpace Administration, South Korea,
e-mail: hjhspace223@gmail.com

ПРОСТОЙ АНАЛИТИЧЕСКИЙ МЕТОД МОДЕЛИРОВАНИЯ УСКОРЕНИЯ ЧАСТИЦ В АСТРОФИЗИЧЕСКИХ УДАРНЫХ ВОЛНАХ С ИСПОЛЬЗОВАНИЕМ УРАВНЕНИЯ ФОККЕРА-ПЛАНКА

Дж.-Х.ХА

Ударные волны часто встречаются в астрофизических средах, и ускорение частиц в астрофизических ударных волнах связано с высокоэнергетическими явлениями. Механизм ускорения и временная эволюция функции распределения частиц тщательно изучены. В этой статье описывается простой аналитический метод с использованием одномерного уравнения Фоккера-Планка в режиме пробных частиц. Основное внимание уделено изучению эволюции функции распределения частиц в ударной волне вверх по потоку, особенно в сценариях, когда частицы могут двигаться к Земле вдоль открытых линий магнитного поля. В работе исследовано поведение аналитического решения в зависимости от различных параметров, характеризующих структуру ударной волны, таких как число Маха ударной волны, бета-плазма, доля инжекции в диффузное ускорение ударной волны и масштаб магнитного поля вверх по потоку. Как и ожидалось, поведение связано с турбулентностью вверх по потоку для диффузионного ускорения ударной волны. Кроме того, предварительно ускоренные частицы могут влиять на временную эволюцию распределения частиц только тогда, когда радиационные или адвективные потери достаточно малы для того, чтобы предварительно ускоренное распределение имело более плоский наклон степенного закона, чем наклон степенного закона, основанный на теории ускорения ударной волны. Кроме того, в статье приводится формула для сферически расширяющейся ударной волны и ее применение для расчета высокоэнергетического излучения в результате адронных взаимодействий. Предположено, что простой аналитический метод может быть эффективно использован для исследования различных типов астрофизических ударных волн, характеризующихся широким диапазоном параметров плазмы.

Ключевые слова: *ускорение частиц: высокоэнергетическое излучение: астрофизические ударные волны: уравнение Фоккера-Планка*

REFERENCES

1. *R.Vainio*, *L.Kocharov*, *T.Laitinen*, Astrophys. J., **528**, 1015, 2000.
2. *T.G.Forbes et al.*, Space Sci. Rev., **123**, 251, 2006.
3. *B.E.Gordon et al.*, Journal of Geophysical Research, **104**, 28263, 1999.
4. *S.P.Reynolds*, Astrophys. Space Sci., **336**, 257, 2011.
5. *G.Morlino*, Nuclear Instruments and Methods in Physics Research Section A: Accelerators, Spectrometers, Detectors and Associated Equipment, **720**, 70, 2013.
6. *A.Bell*, Brazilian Journal of Physics, **44**, 415, 2014.
7. *F.Miniati et al.*, Astrophys. J., **559**, 59, 2001.
8. *D.Ryu et al.*, Astrophys. J., **593**, 599, 2003.
9. *S.E.Hong et al.*, Astrophys. J., **785**, 133, 2014.
10. *J.-H.Ha*, *D.Ryu*, *H.Kang*, Astrophys. J., **857**, 26, 2018.
11. *A.R.Bell*, Mon. Not. Roy. Astron. Soc., **182**, 147, 1978.
12. *R.D.Blandford*, *J.P.Ostriker*, Astrophys. J. Lett., **221**, L29, 1978.
13. *D.Caprioli*, *A.Spitkovsky*, Astrophys. J., **783**, 91, 2014.
14. *J.Park*, *D.Caprioli*, *A.Spitkovsky*, Phys. Rev. Lett., **114**, 085003, 2015.
15. *J.-H.Ha et al.*, Astrophys. J., **864**, 105, 2018.
16. *J.-H.Ha et al.*, Astrophys. J., **915**, 18, 2021.
17. *A.Bodan et al.*, Astrophys. J., **847**, 71, 2017.
18. *R.Xu*, *D.Caprioli*, *A.Spitkovsky*, Astrophys. J. Lett., **897**, L41, 2020.
19. *H.Kang*, *T.W.Jones*, *U.D.J.Gieseler*, Astrophys. J., **579**, 337, 2002.
20. *D.Caprioli et al.*, Mon. Not. Roy. Astron. Soc., **407**, 1773, 2010.
21. *M.A.Malkov*, Astrophys. J., **485**, 638, 1997.
22. *E.Amano*, *P.Blasi*, Mon. Not. Roy. Astron. Soc., **364**, L76, 2005.
23. *H.Kang*, *D.Ryu*, Astrophys. J., **721**, 886, 2010.
24. *J.-H.Ha*, *D.Ryu*, *H.Kang*, Astrophys. J., **892**, 86, 2020.
25. *J.-H.Ha*, *D.Ryu*, *H.Kang*, Astrophys. J., **943**, 119, 2023.
26. *J.-H.Ha*, *D.Ryu*, *H.Kang*, Astrophys. J., **907**, 26, 2021.
27. *E.Peretti et al.*, Mon. Not. Roy. Astron. Soc., **487**, 168, 2019.
28. *E.Peretti et al.*, Mon. Not. Roy. Astron. Soc., 493, 5880, 2020.
29. *M.R.Krumholz et al.*, Mon. Not. Roy. Astron. Soc., **493**, 2817, 2020.
30. *P.H.Yoon*, Physics of Plasmas, **19**, 052301, 2012.
31. *P.H.Yoon*, Journal of Geophysical Research: Space Physics, **119**, 7074, 2014.
32. *V.Pierrard*, *M.Lazar*, S.Stverak, Frontiers in Astron. Space Sci., **9**, 892236, 2022.
33. *R.A.Lopez*, *S.M.Shaaban*, *M.Lazar*, J. Plasma Physics, **87**(3), 905870310, 2021.
34. *M.A.Malkov*, *H.J.Völk*, Advances in Space Research, **21**, 551, 1998.
35. *T.Amano*, *M.Hoshino*, Astrophys. J., **927**, 132, 2022.
36. *A.R.Bell*, Mon. Not. Roy. Astron. Soc., **353**, 550, 2004.
37. *M.A.Riquelme*, *A.Spitkovsky*, Astrophys. J., **694**, 626, 2009.
38. *G.Millward et al.*, Space Weather, **11**, 57, 2013.
39. *H.Kang*, *D.Ryu*, Astrophys. J., **734**, 18, 2011.

40. *P.Mukhopadhyay et al.*, Astrophys. J., **953,** 49, 2023.
41. *F.Acero et al.*, Astrophys. J. Suppl. Ser., **224**, 8, 2016.
42. *A.A.Abdo et al.*, Science, **327**, 1103, 2010.
43. *A.A.Abdo et al.*, Astrophys. J. Lett., **709**, L152, 2010.
44. *S.Abdollahi et al.*, Astrophys. J. Suppl. Ser., **247**, 33, 2020.
45. *A.Abramowski et al.*, Astrophys. J., **757**, 158, 2012.
46. *F.Acero et al.*, Science, **326**, 1080, 2009.
47. *S.R.Kelner*, *F.A.Aharonian*, *V.V.Bugayov*, Phys. Rev. D, **74**, 034018, 2006.